International Journal of Microwave and Wireless Technologies

cambridge.org/mrf

Wideband millimeter-wave reflectarray antenna with reduced cross-polarization

Vidhyashree Sathyanarayanan, Gulam Nabi Alsath Mohammed, Kirubaveni Savarimuthu and Malathi Kanagasabai

Department of Electronics and Communication Engineering, College of Engineering Guindy, Anna University, Chennai, Tamil Nadu, India

Research Paper

Cite this article: Sathyanarayanan V, Alsath Mohammed GN, Savarimuthu K, Kanagasabai M (2024). Wideband millimeter-wave reflectarray antenna with reduced cross-polarization. *International Journal of Microwave and Wireless Technologies* 1–9. https://doi.org/10.1017/S1759078723001587

Received: 28 June 2023
Revised: 6 December 2023
Accepted: 11 December 2023

Keywords:
5G antennas; Array antennas; reflectarray antennas

Corresponding author:
Vidhyashree Sathyanarayanan;
Email:
vidhyashreesathyanarayanan@gmail.com

Abstract

A novel wideband reflectarray antenna (RA) is designed for 5G millimeter (mm) wave communications in the frequency range of 26.5–36 GHz. The proposed unit cell is constructed using a grid periodicity of $0.52\lambda_0$ that offers 636° phase change through phase delay lines (PDLs) (θ_s). These PDLs are attached to the outer end of the unit cell comprising semi-circular rings. Bandwidth enhancement is achieved by incorporating a corrugated slot technique and a suitable air gap beneath the substrate. The proposed center-fed reflectarray is composed of 513 elements distributed in a circular aperture ($13.46\lambda_0$). Using mirror-symmetrical distribution of the unit cells, a cross-polarization reduction as low as −50 dB is realized. At 30 GHz, RA has a measured peak gain of 28.2 dBi, a sidelobe level of −14.3 dB, and an aperture efficiency of 31.4%. The prototype antenna is fabricated, and the simulation results are experimentally validated. The measured 1-dB and 3-dB gain bandwidths of the proposed reflectarray antenna are 31.3% and 41.6%, respectively. The proposed broadband reflectarray can be a potential choice for inter-satellite services like inter-satellite networking/satellite positioning and control; fixed satellite services such as GPS satellite synchronization and data direct to home TV; and satellite position fixing.

Introduction

5G wireless technology has evolved as an emerging technology for applications in mobile broadband wireless services like Earth exploration satellites, fixed satellite services, mobile satellite services, space research services, inter-satellite services, and radio navigation satellites. The connectivity is extremely dependable and secure, enabling easy access to telecommunication services. High data rates, fewer dropped connections, reliability, and efficiency are proficient features of the 5G millimeter wave [1]. Meeting the standards, however, presents several difficulties, including path loss, realizable coverage, and air absorption of electromagnetic waves. Reflectarray antennas (RAs) with desirable characteristics like high gain, flexible mounting, and planar structure are well suited for 5G millimeter wave frequencies [2, 3] to meet these requirements. For 5G communications, the bandwidth of traditional RA needs to be increased to handle more data.

Several researchers have attempted to design performance-enhanced RAs covering the X-band to K-band [4–6] spectrum. Techniques such as vertical slide tilting [7], dielectric resonator height variations [8], log periodic structures [9], sub-wavelength elements [10], polarization converters [11], and windmill structures [12] offer narrower bandwidths up to 10%. The limitation in bandwidth performance is attributed to the dependency on single or dual resonance methods. To improve bandwidth, researchers have combined two or more techniques to broaden the antenna bandwidth. This includes the combination of multi-resonance unit cells with an additional air gap [13] and multi-layer solutions utilizing sub-wavelength elements [14]. The combined bandwidth enhancement techniques offered bandwidth enhancement of up to 19%. Liu et al., in their study [15], inherited two different resonant structures in alternating zones of a single-layer reflectarray to widen the bandwidth. The antenna design is accomplished using the spatial compensation technique.

The unit cell used in the study by Suresh et al. [16], operating at 26.5 GHz, consists of concentric coupled square structures with delay lines positioned in orthogonal directions. The reported unit cell provides an improved phase span of 420°. This center-fed reflectarray with 413 elements provides a maximum gain of 27.1 dBi and a 1 dB gain bandwidth of 28.6%. In [17], a single-layer reflectarray containing a unit cell with a square ring and a square patch that has been turned 45° provides a 450° phase range with a 20° phase error in the limited frequency range. The combined use of the air gap and the optimized 1296 patch components results in a 1 dB gain bandwidth of 29.3% at 45 GHz. In the study by Wu et al. [18], a single-layer, low-cost, wideband reflectarray

with linear polarization is reported. The 180° reflection phase difference between the two states for the unit cell is obtained by switching the ground-signal-ground transmission line between "open" and "short" to the ground. The reported reflectarray offers 32% bandwidth with reference 1.5 dB gain.

To reradiate electromagnetic waves in phase as a planar wave, Mohammad and Hassan, in their study [19], present a reflectarray utilizing the phase delay lines (PDLs). Frequency selective surface structures of the two-layer square-loop type are used to implement the radiating elements in each zone. The proposed reflectarray achieves a 40% fractional bandwidth with a gain of 26.42 2 dB in the Ku-band. Zheng et al., in their study [20], present a waveguide-type reflectarray comprising dielectric posts embedded with four identical copper wires, providing a phase range of around 400° at 30 GHz. The simulation results of the antenna achieve pencil beamwidth with a sidelobe of −20 dB using 256 elements. Furthermore, the simulated maximum efficiency and gain results are 49.98% and 23 dB, respectively. A double-layer element with a spider-shaped unit cell [21] is used to develop a wideband reflectarray with low cross-polarization and a large phase variation of 800°. The reported offset-fed reflectarray with 6769 elements with octagonal aperture has 1- and 3-dB gain bandwidths of 25.2% and 32.3%, respectively, with an operating frequency range of 10–13.85 GHz. Cross-polarization values of less than 40 dB and a peak gain of 31.2 dBi are obtained with an aperture efficiency of 42%.

In this work, hybrid approaches, namely multi-resonant and air gap insertion techniques, improve the RA's bandwidth performance. A pair of circular loops with an embedded corrugated slot make up the unit cell that is being displayed. It has a linear phase response of 636° and a unit cell bandwidth of 65.6%. By properly designing a unit cell that produces closely spaced parallel phase curves throughout the targeted frequency range, the bandwidth increase is accomplished. With 513 components, the manufactured RA has a measured peak gain of 28.2 dB, a 1 dB gain bandwidth of 31.3%, and an aperture efficiency of 52.4%. The introduction of a unique mirror-symmetry configuration reduces cross-polarization by up to −50 dB. Therefore, the proposed RA exhibits a wider bandwidth, better radiation performance, and reduced cross-polarization. The rest of the paper is organized as follows: "Design and analysis of unit cell" section describes the unit cell's construction and detailed parametric investigation; "Reflectarray design and analysis" section details the proposed reflectarray construction and array optimization along with the radiation characteristics; and finally, the gain, aperture efficiency calculation, and performance comparison with existing work are detailed in the "Results and discussion" section.

Design and analysis of unit cell

Unit cell design

The geometry of the proposed unit cell is illustrated in Fig. 1. The unit cell consists of two semi-circular rings coupled through a narrow horizontal slot. The radius of the concentric rings in the unit cell follows an iterative logic to achieve the necessary phase swing. The outermost ring is given by the factor $C_0 = C_{in} + (4 \times w_0)$, while the middle ring is expressed as $C_m = C_{in} + (2 \times w_0)$. The gap and width of the rings are fixed as $g_o = g_m = 0.3$ mm. To these rings, phase-compensating PDLs are attached to the outer periphery, as described in Fig. 1. The length of the PDLs is adjusted to meet the necessary phase compensation requirements during the design of the RA. The unit element with a grid periodicity of $0.52\lambda_0$ is developed on RT Duroid 5870 substrate with height $h_1 = 0.254$ mm and relative permittivity ε_r value as 2.33 with tan δ as 0.0012. The proposed unit cell has a full conductive ground, as shown in Fig. 1(b), supported by FR4 substrate thickness of $h_2 = 0.8$ mm. For smoother and more dynamic reflection phase response and mechanical stability, 2 mm polyurethane is loaded between the substrate and the ground. The proposed element design is characterized using Floquet ports with periodic boundary conditions using CST Studio Suite.

Evolution

In this research, phase range enhancement is achieved with concentric ring elements, as described by Veluchamy et al. [22]. Unlike [22], the evolution of the proposed reflectarray element starts with coupled half-circular rings, as shown in the inset of Fig. 2 (referred to as Cell 1). The spacing between the half-circular rings is carefully adjusted to induce coupling between the top and bottom circular rings. Two arc-shaped PDLs are represented as (θ_s), systematically connected to the outermost half-circular ring to achieve the desired phase compensation. The phase characterization using the Floquet boundary condition indicates that the coupled half-circular rings

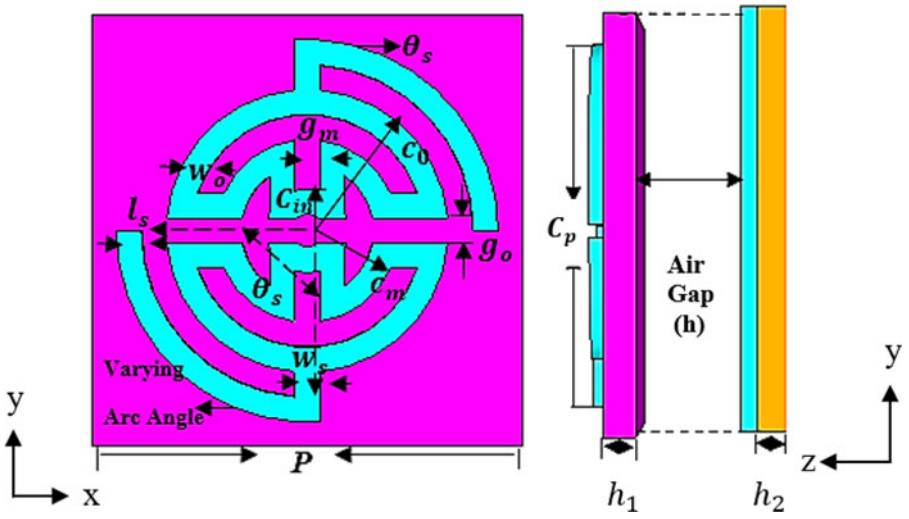

Figure 1. Layout of the reflectarray proposed unit cell: (a) front view and (b) side view.
Note: cyan denotes metal; pink denotes RT Duroid substrate; and brown denotes FR4 substrate.

https://doi.org/10.1017/S1759078723001587 Published online by Cambridge University Press

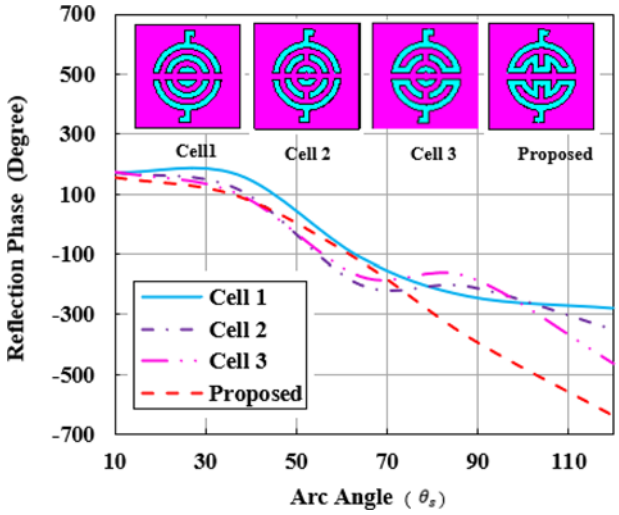

Figure 2. Reflection phase characteristics during the evolution stages.

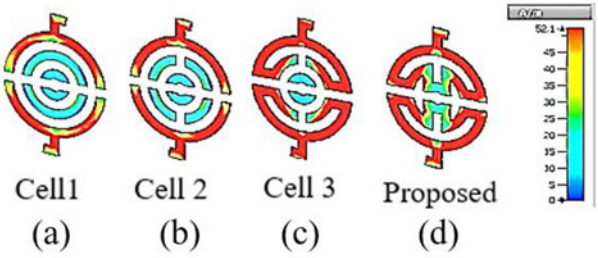

Figure 3. Evolution of the proposed element through surface current distribution. (a) Unit cell 1; (b) Unit cell 2; (c) Unit cell 3; and (d) Proposed.

provide a reflection phase range of 380° corresponding to a reflection bandwidth of 29%. To further enhance the phase variations, a vertical slit of width g_m is introduced in the middle ring as evident in Cell 2 of Fig. 2. The resultant configuration has an improved phase span of 450° along with a reflection bandwidth of 32%.

However, the Cell 2 phase response is limited by the fact that the element produces a steep phase variation. The current distribution plot of the proposed antenna, as shown in Fig. 3(a–b), reveals that the propagating current in the reflectarray element is highly localized to the outermost ring. Hence, distributing the current throughout the aperture of the element would significantly improve the phase characteristics of the reflectarray element. Thus, to control the phase slope, the outer and the middle rings are connected using short stubs as in Cell 3. The localized surface currents on the outer ring of the reflectarray element find an additional current path (Fig. 3(c)), leading to a gradual phase variation of 539°, as shown in Fig. 2. Further improvement in current propagation characteristics is achieved by interconnecting the middle and the innermost rings, as described in Fig. 3(d). The final geometry has a convoluted structure with a phase range improvement of 636°. The corresponding reflection bandwidth is estimated to be 65.6%. Figure 4 illustrates the proposed unit cell reflection phase characteristics varying as a function of arc length (θ_s) with a reflection magnitude less than −0.48 dB. Thus, from the study of the unit cell characteristics, it is inferred that the proposed reflectarray element combines three resonant modes to achieve a wider reflection bandwidth. The optimized dimensions of the unit cell are given in Table 1.

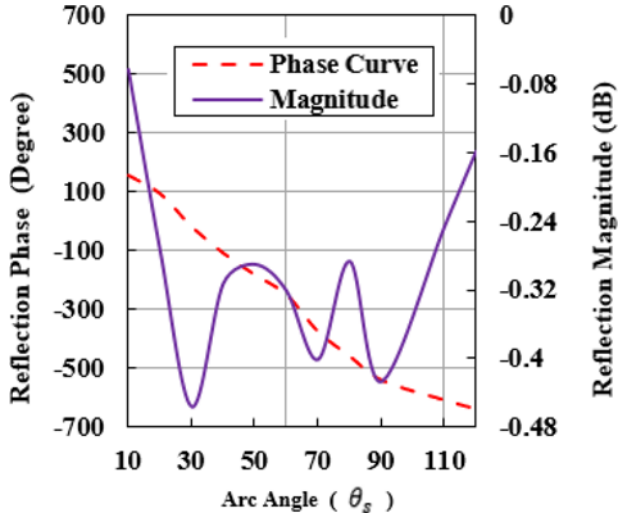

Figure 4. Reflection phase characteristics as a function of varying arc angle (θ_s).

Table 1. Geometrical parameters of the proposed unit cell

Parameters	θ_s	C_{in}	C_m	C_o	g_m, g_0	h_1	h_2	w_o, w_s	l_s	P
Value (mm)	(10–120)°	0.5	1.1	1.7	0.3	0.25	0.8	0.3	0.3	5.2

Effect of the air gap and dielectric constant

To verify the unit cell characteristics, parametric analysis is performed for varying thicknesses and different dielectric constants of the microwave laminate. The variation in the air gap "h" produces a drastic impact on phase range. For $h = 2$ mm, 636° even phase variation with reduced phase slope is achieved. With $h = 3$ mm, the phase range decreases by 100° along with a larger phase slope. When the substrate thickness is increased to 4 mm, a 400° phase span with a steep slope is observed. Hence, the 2 mm air gap is fixed as a compromise between the gradual phase slope and large reflection phase response, as shown in Fig. 5(a). The next investigation was attempted on the impact of the dielectric material parameters on the phase response. The unit cell with a thick substrate offers a low-phase range and a wider bandwidth. The substrate with low permittivity ($\varepsilon_r = 2.2$) is chosen as it offers a smaller phase slope of 72°/mm and an improved phase range, as shown in Fig. 5(b).

Parallel phase slopes and incident angle effect

To analyze the performance of the proposed element concerning bandwidth, the phase span is observed for various frequencies from 26.2 to 37.1 GHz by varying the values of θ_s, as shown in Fig. 5(c). It is observed that the designed unit cell offers minimal space parallel phase span for the frequency range from 26.5 to 36 GHz, making it suitable for wideband performance in comparison with [17, 23]. The angular and polarization stability of the unit cell is investigated for different angles in steps of 15° and 25° for θ and ϕ planes, respectively. The unit cell remained insensitive to both TE and TM modes of operation within the acceptable phase deviation up to 20°, as shown in Fig. 5(d). The simulated reflected phase of the proposed element for varying arc lengths from 10° to 120° in the frequency range between 23 and 40 GHz is illustrated in Fig. 6. From the figure, it is inferred that the reflected phase

https://doi.org/10.1017/S1759078723001587 Published online by Cambridge University Press

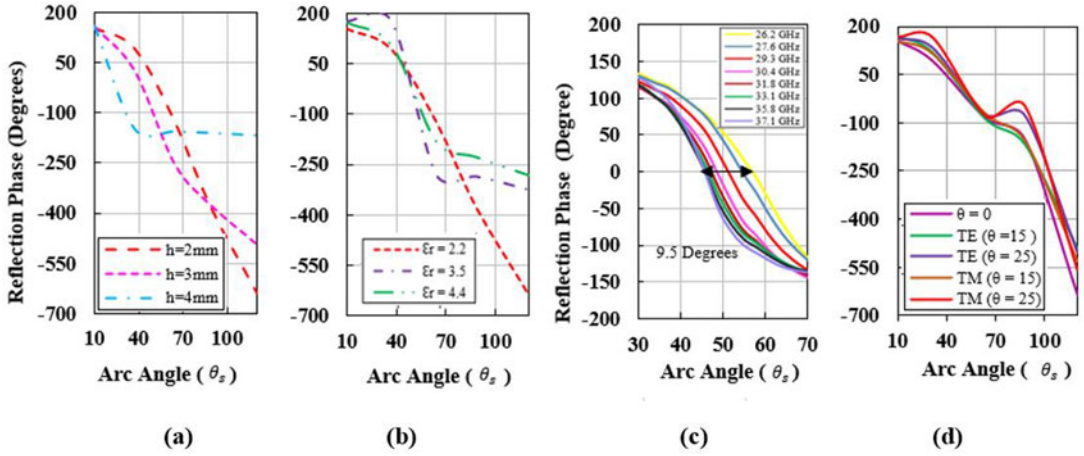

Figure 5. Reflection phase vs. varying arc angle (θ_s) (a) for varied air gap (h), (b) for varied dielectric permittivity (ε_r), (c) for different frequencies in Ka-band, and (d) for different angle of incidence in Transverse Electric (TE) and Transverse Magnetic (TM) modes.

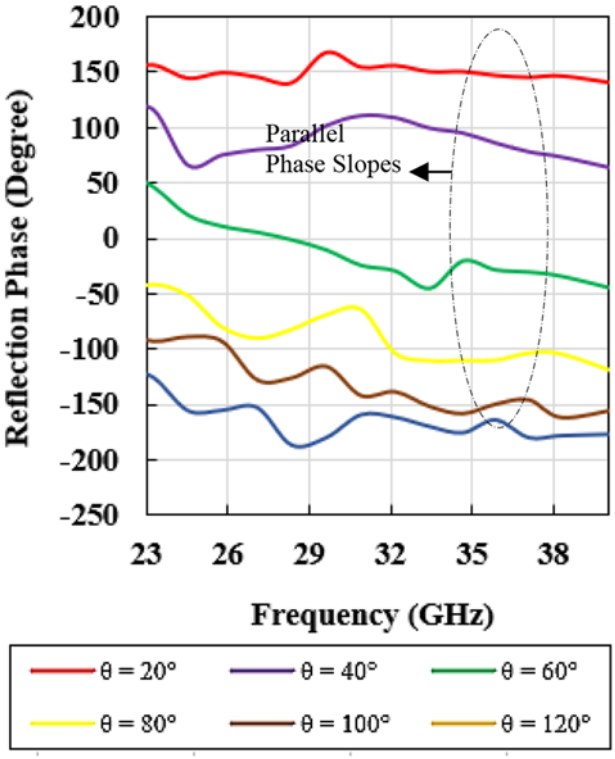

Figure 6. Reflection phase vs. varying arc angle (θ_s) at different frequencies.

curve of the proposed unit cell is a linear parallel phase range concerning frequency, thus justifying the bandwidth improvement. Therefore, parametric analysis and parallel phase slope designate this RA to be suitable for large-sized and offset-fed reflectarray applications.

Reflectarray design and analysis

Based on optimized unit cell elements, a wideband RA ($13.46\lambda_0 \times 13.46\lambda_0$) with 513 elements is built to operate at the center frequency of 30 GHz. The reflectarray is first constructed using a rectangular aperture with 625 elements. Equation (1) is used to calculate the phase compensation required for each element in the reflectarray configuration [15].

$$\Phi_{mn(r)} = k_0(d_i - (x_i\cos\Phi_0 + y_i\sin\Phi_0) \times \sin\theta_0) \quad (1)$$

where k_0 is the propagation constant in free space, d_i is the separation between the midpoint of ith element (x_i, y_i) of the developed RA to the midpoint of the antenna source, and (θ_0, ϕ_0) is the primary beam direction. The calculated phase distribution of the reflectarray construction is given in Fig. 7(a).

The RA uses 18–40 GHz pyramidal horn with a flare length of 20.5 mm as a feed source with an average gain of 15 dB in both the principal planes. The measured radiation pattern of the K/Ka-band standard pyramidal horn is shown in Fig. 7(b). The 1 dB bandwidth achieved from 26.5 to 35 GHz was obtained utilizing 513 elements. At higher frequencies between 33.1 and 37.1 GHz, a steep slope is observed. To mitigate this steep slope, a constant reference phase ($\Delta\Phi_1$) = 25° is added to the 33.1 GHz phase curve elements. By using this procedure, the overall performance of the reflectarray is changed. This 25° constant phase change was fixed with a parametric analysis procedure [24], as shown in Fig. 8. For different reference phase values of 15°, the gain of the higher frequency range increased, whereas in the case of 35°, the gain drastically reduced, where 1 dB bandwidth was not achieved compared with 25°. The addition of the reference phase to the existing phase values is given by Equation (2). Hence, by applying 25°, the phase slope tends to be gradual, which contributes to the parallel phase slope.

$$\Phi_{mn(r)}(\Delta\Phi_1) = \Phi_{mn(r)} + \Delta\Phi_2 \quad (2)$$

where $\Phi_{mn(r)}(\Delta\Phi_1)$ is given by the required phase range with the addition of a constant reference phase and $\Phi_{mn(r)}$ is the required phase range.

Furthermore, the phase error function is calculated as the difference between the achievable reflection phase and the required phase range [25] and is given by Equation (3).

$$PE_{mn} = \left|\Phi_{mn(a)} - \Phi_{mn(r)}(\Delta\Phi_1)\right| \quad (3)$$

where PE_{mn} is the phase error function and $\Phi_{mn(a)}$ is the achieved phase range.

By using the addition of a constant phase reference technique, this phase error function is to be minimized, thereby leading

https://doi.org/10.1017/S1759078723001587 Published online by Cambridge University Press

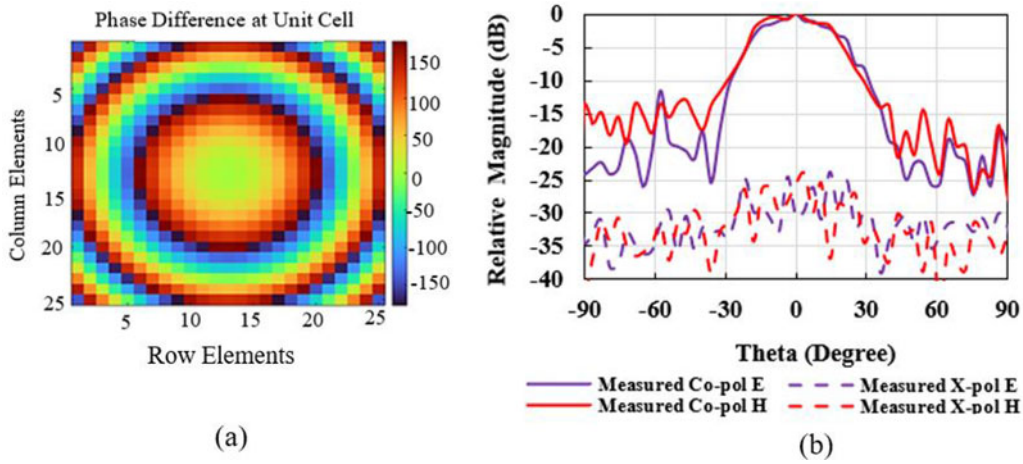

Figure 7. (a) Phase distribution of the proposed array. (b) Measured radiation pattern of K/Ka-band feed horn.

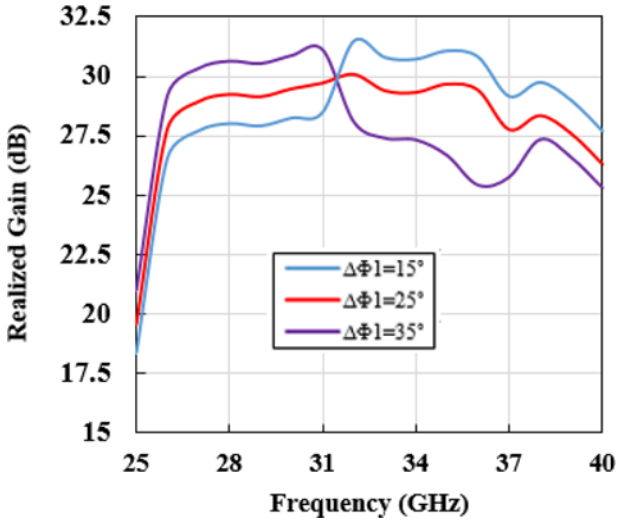

Figure 8. Simulated gain performance by adding a constant reference phase.

to a 1 dB wider bandwidth. To attain maximum aperture efficiency, the footprint of its feed should not be extended more or less than the aperture area. A circular-shaped reflector is preferred for the proposed center-fed reflectarray to achieve high aperture efficiency. To reduce cross-polarization, a special arrangement is adopted in which the reflector is divided into four quadrants, and each quadrant is mirror-symmetrical to one along the x and y directions. Because the surface currents are oppositely directed for the neighboring elements, the transverse currents are canceled in the far field, thereby reducing cross-polarization [26], as shown in Fig. 11(a). The photograph of the fabricated prototype in the test setup is shown in Fig. 11(b). The distance between the source K/Ka-band pyramidal horn and the reflector is maintained at 140 mm, considering the focal distance to diameter (f/D) ratio as 1. The fabricated RA is measured in the $7 \times 3 \times 3$-m anechoic chamber using an N9917A microwave analyzer for observing the radiation and gain plot characteristics.

After reflectarray construction, the square aperture geometry consists of 625 elements. The outer edge elements contribute to increased sidelobe level for radiation pattern formation. Hence, a circular aperture is designed in which the 28 corner elements in each quadrant with the total number of elements as 112 from 625 elements are omitted and gain is improved up to 0.5 dB compared to square aperture reflectarray, as shown in Fig. 9. Thus, by using the optimization procedure, the gain of the reflectarray is improved to 28.2 dBi. Typically, a circular footprint is projected onto the antenna aperture surface for the center feed. The area illuminated by a feed within its intended 3 dB beamwidth coverage on the surface of a reflectarray is referred to as the feed's footprint. To maximize efficiency for a reflectarray, the footprint must be identical as shown in the study by Dahri et al. [25]. The circular shaped aperture is chosen to achieve maximum aperture efficiency combined with selecting an acceptable feed distance where $f/D = 1$, as illustrated in Fig. 12(e) based on this center feed footprint behavior. To improve the cross-polarization performance, PDLs attached to the unit cell are reoriented, as described in Fig. 10. The fourfold symmetrical reflectarray aperture is converted into mirror-symmetrical to enhance the cross-polarization performance, as described in Fig. 10. The vector current distribution of the proposed RA is shown in Fig. 11. From the figure, it can be inferred that the current cancellation occurs between the mirror-symmetrically oriented PDLs in the proposed reflectarray geometry. The currents in the PDL get canceled in each quadrant, thereby reducing the cross-polarization.

Results and discussion

The simulated and measured E and H plane radiation patterns and cross-polarization depict consistency in the radiation pattern at almost all frequencies ranging from 26.5 to 36 GHz, as shown in Fig. 12(a–d). The experimental 1 dB and 3 dB gain bandwidths of 31.3% and 41.6% along with a peak gain of 28.2 dBi are shown in Fig. 12(e). The variations between the measured and simulated results are attributed to the cable loss factor. The aperture efficiency is given by Equation (4), and the peak aperture efficiency of the proposed reflectarray is 31.4% at 30 GHz.

$$A_{eff} = \frac{G\lambda^2}{4\pi} \tag{4}$$

The optimal trade-off between aperture efficiency, spillover, and feed blockage is obtained by choosing the right f/D ratio. The small f/D value results in spillover loss, while high aperture efficiency is achievable for f/D ratio in the range of 0.7–1 [25, 27, 28].

https://doi.org/10.1017/S1759078723001587 Published online by Cambridge University Press

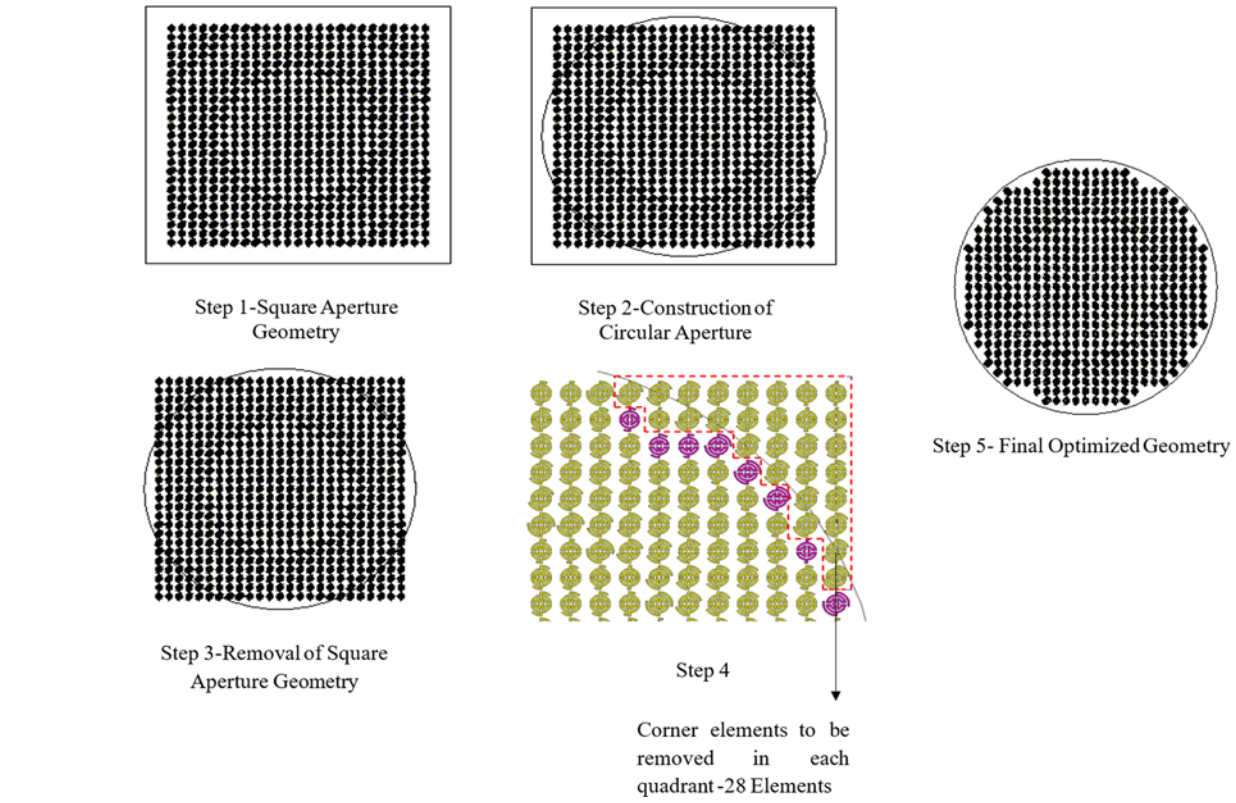

Figure 9. Optimization procedure of conversion from square aperture geometry to circular aperture geometry.

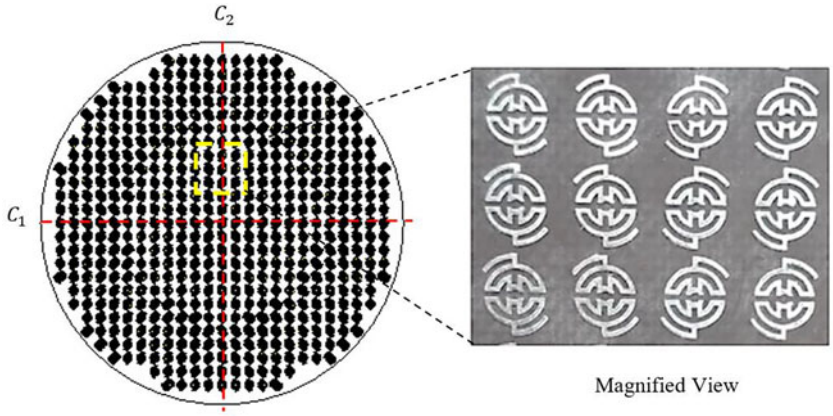

Figure 10. Mirror-symmetry arrangement to reduce cross-polarization effect.

For $f/D = 0.8$, the 1 dB gain bandwidth is 26.6%, and an aperture efficiency of 39.23% is achieved. Similarly, for $f/D = 1$, 1 dB gain bandwidth and peak aperture efficiency are reported as 31.3% and 31.4%, respectively, as shown in Fig. 12(e). Since the bandwidth and aperture efficiency for $f/D = 1$ are high comparably, the focal distance between the array and horn is maintained as 140 mm. Table 2 provides 1 dB gain bandwidth and aperture efficiency values for different f/D ratios. Table 2 imparts the proposed reflectarray performance comparison with earlier research works.

The following are some of the advantages of the present research over the previous works:

1. In comparison with the unit cell structures presented in [8, 9, 12, and 16], the proposed unit cell configuration offers an increased phase span of 636° covering the frequency range of 26.5–36 GHz.
2. The novel RA structure affords a better 1 dB gain bandwidth of 31.3%, covering the bandwidth from 26.5 to 36 GHz, compared to other structures reported in [4–16].
3. Using the mirror-symmetry technique, the cross-polarization is reduced to <−50 dB in comparison with other literature reported in [6, 8, 9, and 12].
4. The fabricated RA offers 28.2 dBi peak gain in comparison with the research reported in [4, 9, 11, and 23] and 31.4% aperture efficiency when compared to [4] and [11] using only 513 elements.
5. In comparison with work by Zhao et al. [9], the current work is better in terms of phase span ranging over 636°, gain of 28.2 dB,

https://doi.org/10.1017/S1759078723001587 Published online by Cambridge University Press

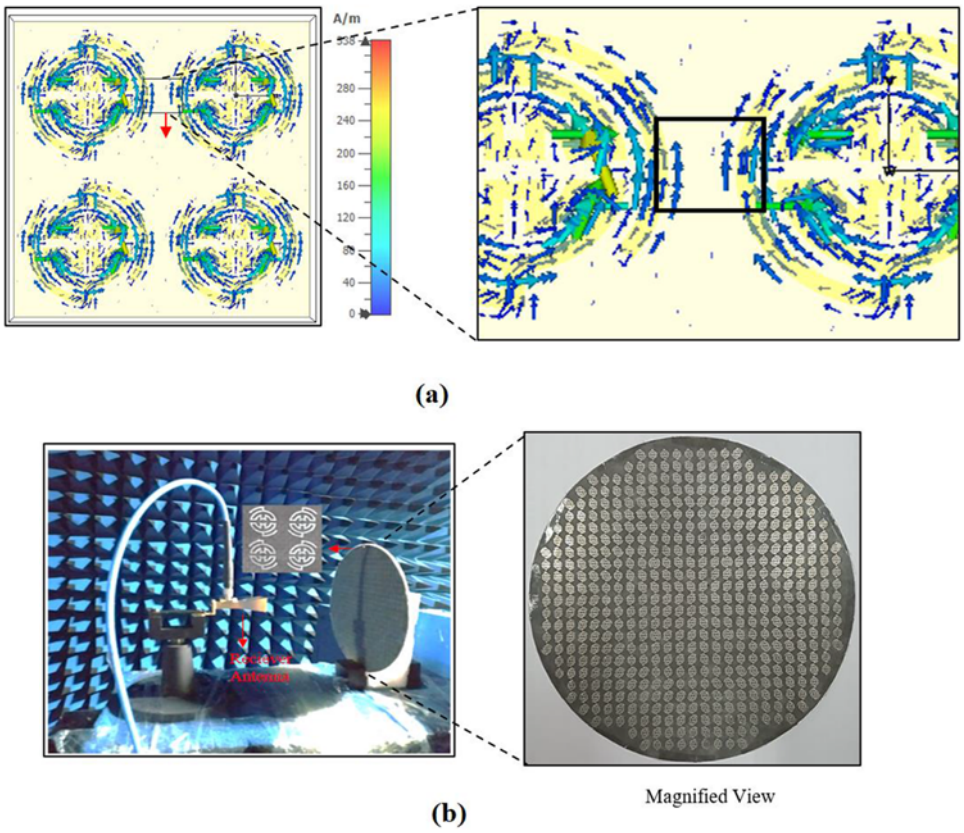

Figure 11. (a) Surface current distribution of the reflectarray structure. (b) Proposed reflectarray in the measurement setup.

Table 2. Performance comparison with similar works

Parameters	Current work	[9]	[7]	[8]	[12]	[16]
Resonating freq. (GHz)	30	33	26	30	37	26.5
Phase span (°)	636	360	650	360	473	420
Total elements	513	324	332	625	400	413
Aperture size (λ_0)	13.46	9	6.80	12	6.93	12.5
Gain (dBi)	28.2	26.6	24.4	28	27.8	27.1
1 dB Gain BW (%)	31.3	10.6	6.1	10	18.6[a]	28.6
SLL (dB)	<−14.3	<−17.8	<−16	<−25.5	<−17.9	<−14.5
X-Pol. level (dB)	<−50	−15	−19	−30	<−25	<−28
3 dB Beamwidth	6.2	6.6	6	7	NR	5.7
Peak aperture efficiency (%)	31.4	46.3	28	NR	51.7	51.2
f/D ratio	1	0.9	0.8	1	1	1

NR = Not reported.
[a]1 dB gain bandwidth (BW), SLL: Side Lobe Level.

1 dB gain bandwidth of 31.3%, and cross-polarization less than 50 dB.

Therefore, the developed RA structure operates at 5G communication satellite frequencies by inheriting characteristics like narrower beamwidth, enhanced bandwidth performance, and a reduction in cross-polarization levels.

Conclusion

Improved gain, circular aperture-printed wideband RA has become a proactive element for 5G satellite frequency applications. The proposed element ($0.52\lambda_0$) constitute a corrugated circular ring structure that offers a phase span of 636° and a unit cell reflection bandwidth of 65.6%. Based on an optimized unit cell, a circular aperture ($13.46\lambda_0$) feed center-oriented reflectarray is developed and constructed at a resonating frequency of 30 GHz.

https://doi.org/10.1017/S1759078723001587 Published online by Cambridge University Press

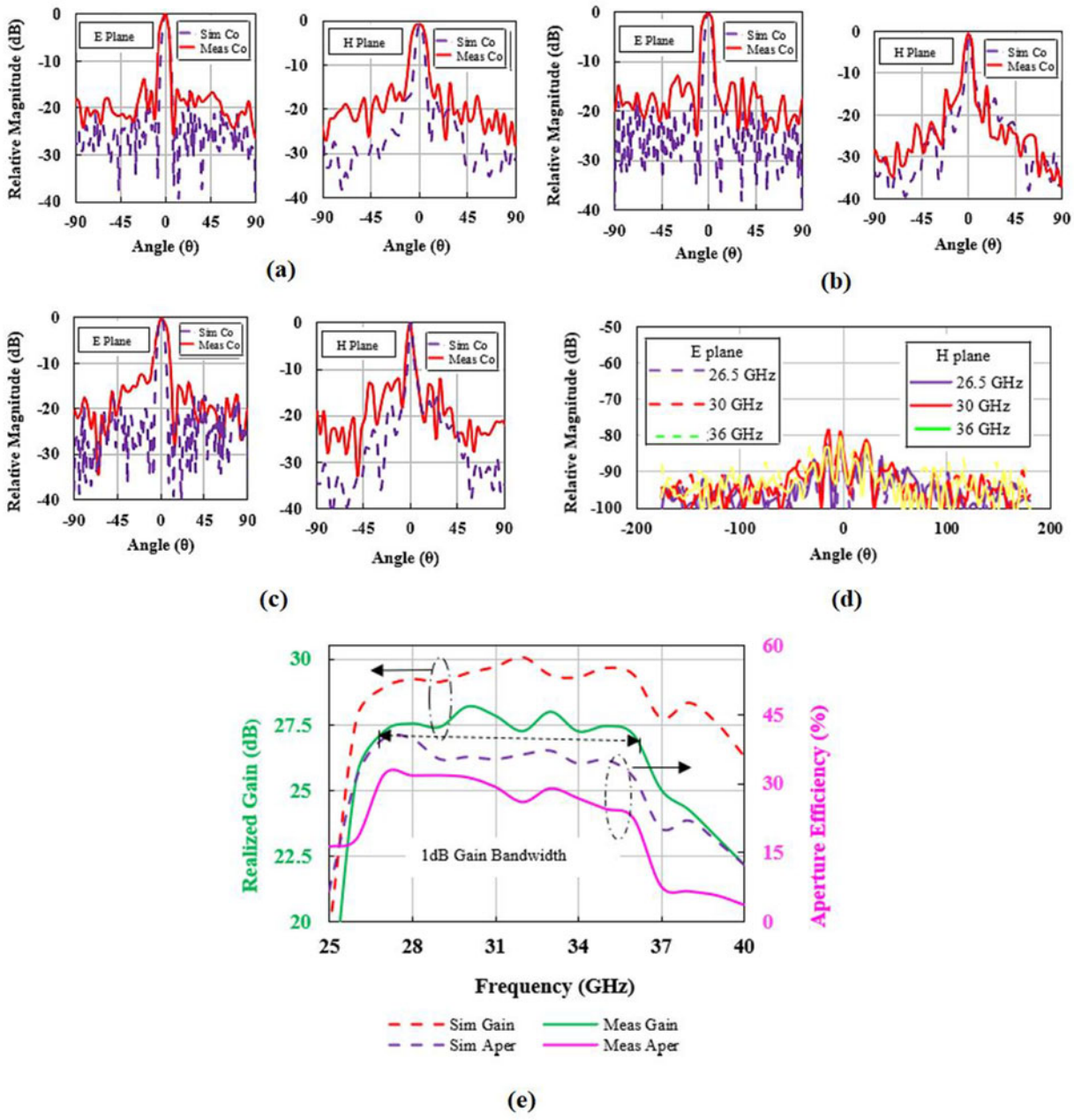

Figure 12. Normalized E and H plane radiation patterns at different frequencies: (a) 26.5 GHz, (b) 30 GHz, and (c) 36 GHz. (d) Cross-polarization characteristics. (e) Gain and aperture efficiency characteristics.

The experimental findings demonstrate that an aperture efficiency >26% throughout the frequency range and a bandwidth of 31.3% of 1 dB gain bandwidth are achieved with 513 elements. By inheriting the mirror-symmetry technique, cross-polarization has been reduced up to −50 dB at 30 GHz. Thus, the proposed reflectarray offering 31.3% wide 1 dB gain bandwidth performance is well suited for various 5G satellite communications like Earth exploration satellite services, radio astronomy services, and radar altimeters (sea level measurements).

Competing interests. The authors report that there is no conflict of interest.

References

1. **Rappaport TS, Xing Y, Mac Cartney GR, Molisch AF, Mellios E and Zhang J** (2017) Overview of millimeter-wave communications for fifth-generation (5G) wireless networks – with a focus on propagation models. *IEEE Transactions on Antennas and Propagation* **65**(12), 6213–6230.
2. **Dahri MH, Jamaluddin MH, Abbasi MI and Kamarudin MR** (2017) A review of wideband reflectarray antennas for 5G communication systems. *IEEE Access* **5**, 17803–17815.
3. **Kavitha N, Gulam Nabi Alsath M, Kirubaveni S, Ramprabhu S and Malathi K** (2020) A comprehensive analysis on the state-of-the-art developments in reflectarray, transmitarray, and transmit-reflectarray antennas. *International Journal of RF and Microwave Computer-Aided Engineering* **30**(9), e22272.
4. **Veluchamy L, Mohammed G, Krishnasamy T and Jyoti R** (2019) A wideband, single layer reflectarray antenna with cross loop and square ring slot loaded patch elements. *International Journal of Microwave and Wireless Technologies* **11**(7), 703–710.
5. **Encinar JA, Florencio R, Arrebola M, Natera MAS, Barba M, Page JE, Boix RR and Toso G** (2018) Dual-polarization reflectarray in Ku-band

https://doi.org/10.1017/S1759078723001587 Published online by Cambridge University Press

based on two layers of dipole arrays for a transmit–receive satellite antenna with South American coverage. *International Journal of Microwave and Wireless Technologies* **10**, 149–159.
6. **Suresh V** (2023) Optimum design of a novel electronically reconfigurable reflectarray antenna for X/Ku band applications. *Journal of High-Frequency Communication Technologies* **1**, 12–23.
7. **Dahri M, Jamaluddin MH, Seman F, Inam M, Ashyap A, Kamarudin M and Hayat O** (2020) A novel asymmetric patch reflectarray antenna with ground ring slots for 5G communication systems. *Electronics* **9**, 1450.
8. **Zhang S** (2017) Three-dimensional printed millimeter wave dielectric resonator reflectarray. *IET Microwaves, Antennas & Propagation* **11**, 2005–2009.
9. **Zhao J, li H, Zhou Y, Wang H, Tianming L, Biao H and Zou H** (2020) A single-layer Ka-band broadband reflectarray antenna using log-periodic elements. *Microwave and Optical Technology Letters* **62**(1), 371–377.
10. **Nayeri P, Yang F and Elsherbeni A** (2011) Bandwidth improvement of reflectarray antennas using closely spaced elements. *Progress In Electromagnetics Research C* **18**, 19–29.
11. **Yu Z-Y, Zhang Y-H, He S-Y, Gao H-T, Chen HT and Zhu G-Q** (2022) A wide-angle coverage and low scan loss beam steering circularly polarized folded reflectarray antenna for millimeter-wave applications. *IEEE Transactions on Antennas and Propagation* **70**(4), 2656–2667.
12. **Zhao J, Fu C, Li H, Li F and Hu X** (2022) A single-layer broadband Ka-band reflectarray using novel windmill elements. *IEEE Transactions on Antennas and Propagation* **70**(11), 11167–11171.
13. **Vosoogh A, Keyghobad K, Khaleghi A and Mansouri S** (2014) A high-efficiency Ku-band reflectarray antenna using single-layer multi-resonance elements. *IEEE Antennas and Wireless Propagation Letters* **13**, 891–894.
14. **Nayeri P and Elsherbeni A** (2010) Broadband reflectarray antennas using double-layer subwavelength patch elements. *IEEE Antennas and Wireless Propagation Letters* **9**, 1139–1142.
15. **Liu Y, Cheng Y, Lei X and Kou P** (2018) Millimeter-wave single-layer wideband high-gain reflectarray antenna with ability of spatial dispersion compensation. In *IEEE Transactions on Antennas and Propagation*, 1–1.
16. **Suresh V, Mohammed GNA and Narayanasamy K** (2022) A novel broadband reflectarray for 5G satellite communications. *The International Journal of RF and Microwave Computer-Aided Engineering* **32**(2), e22972.
17. **Xia X, Wu Q, Wang H, Yu C and Hong W** (2017) Wideband millimeter-wave microstrip reflectarray using dual-resonance unit cells. *IEEE Antennas and Wireless Propagation Letters* **16**, 4–7.
18. **Wu W, Xu D, Chen Q, Tanaka T and Kozai M** (2022) A wideband reflectarray based on single-layer magneto-electric dipole elements with 1-bit switching mode. *IEEE Transactions on Antennas and Propagation* **70**(12), 12346–12351.
19. **Mohammad A and Hassan A** (2022) Ultra-wideband reflectarray antenna using two layers square-loop frequency selective surfaces. *Progress In Electromagnetics Research C* **118**, 43–59.
20. **Zheng Z, Zhang L, Luo Q, Mao C and He Y** (2022) A wideband reflectarray antenna for millimeter-wave applications. In *2022 IEEE 10th Asia-Pacific Conference on Antennas and Propagation (APCAP)*, Xiamen, China, 1–2.
21. **Elahi M, Jeong T, Yang Y, Lee K-Y and Hwang KC** (2023) A wideband reflectarray antenna for satellite application with low cross-polarization. *Applied Sciences* **13**, 4545.
22. **Veluchamy L, Selvan KT, Jyoti R and Sravan Kumar S** (2023) Wideband reflectarray antennas using concentric ring-based elements for Ku band applications. *IETE Journal of Research* **69**(3), 1675–1685.
23. **Sharifi R, Basiri R and Zareian-Jahromi E** (2020) Optimization-based design of a single-layer wideband reflectarray antenna in the terahertz regime. *Journal of Computational Electronics* **19**(1), 469–481.
24. **Mao Y, Xu S, Yang F and Elsherbeni AZ** (2015) A novel phase synthesis approach for wideband reflectarray design. *IEEE Transactions on Antennas and Propagation* **63**(9), 4189–4193.
25. **Dahri M, Jamaluddin MH, Seman F, Inam M, Sallehuddin N, Ashyap A and Kamarudin M** (2020) Aspects of efficiency enhancement in reflectarrays with analytical investigation and accurate measurement. *Electronics* **9**, 1887.
26. **Li X and Yang L** (2020) Single-layer dual-band wide band-ratio reflectarray with orthogonal linear polarization. *IEEE Access* **8**, 93586–93593.
27. **Jamaluddin MH, Gillard R, Sauleau R, Koleck T, Castel X, Benzerga R and Le Coq L** (2010) Dielectric resonator antenna reflectarray in Ka-band. In *2010 IEEE Antennas and Propagation Society International Symposium*, 1–4.
28. **Narayanasamy K, Mohammed GNA, Savarimuthu K, Sivasamy R and Kanagasabai M** (2021) A novel Ku/K band reflectarray antenna with reduced phase slope and phase sensitivity. *The International Journal of RF and Microwave Computer-Aided Engineering* **31**(7), e22699.

https://doi.org/10.1017/S1759078723001587 Published online by Cambridge University Press